Langmuir

Article

pubs.acs.org/Langmuir

Creating Controlled Thickness Gradients in Polymer Thin Films via Flowcoating

Raleigh L. Davis,[†] Sahana Jayaraman,[†] Paul M. Chaikin,[‡] and Richard A. Register*[,†]

[†]Department of Chemical and Biological Engineering and Princeton Institute for the Science and Technology of Materials, Princeton University, Princeton, New Jersey 08544, United States

[‡]Department of Physics, New York University, New York, New York 10003, United States

Supporting Information

ABSTRACT: Flowcoating is a popular technique for generating thin (5−200 nm), substrate-supported polymer films. In this process, a reservoir of coating fluid is held between the horizontal substrate and a nearly horizontal blade above the substrate; a film of fluid is drawn out of the reservoir by moving the substrate. Accelerating the substrate produces a film with a thickness gradient, particularly useful for high-throughput measurements where film thickness is an important parameter. The present work compares experimental film thickness profiles with a model based on a Landau−Levich treatment to identify the experimental parameters which govern film thickness. The key parameters are the capillary number and the radius of curvature of the reservoir's static meniscus, which is set by the blade angle, gap height, solution reservoir volume, and contact angles of the fluid with the blade and substrate. The results show excellent quantitative agreement with the first-principles model; the model thus provides a design approach which allows a user to produce polymer thin films of virtually any desired thickness profile.

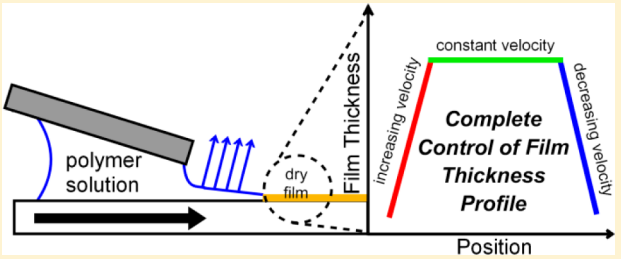

INTRODUCTION

Creation of thin (<200 nm) polymer films is a subject of intense interest, with applications in fields such as medicine,[1,2] optics,[3] and microelectronics.[4,5] Numerous methods exist to deposit thin polymer films including spin-coating,[6] dip-coating,[7] layer-by-layer assembly,[8] and physical,[9] chemical,[10] and laser deposition.[11] An additional method, invented by Stafford et al. and titled flowcoating, has the useful advantage of being able to generate both flat films and films which possess a thickness gradient.[12] The basic setup of a flowcoater is displayed in Figure 1. To produce a film, polymer solution is placed between a fixed blade and a substrate which rests upon a programmable translation stage. Once the solution is in place, the stage is made to move, gradually drawing solution from the reservoir and producing a film on the substrate with thickness t_{wet}. If the stage accelerates, solution is drawn out at a disproportionately faster rate, leading to a greater t_{wet}. The solvent then evaporates, leaving behind a dry polymer film of thickness t_{dry}. Because of the technique's ease of use and potential for integration into large-scale production methods,[13] numerous efforts have utilized this approach for deposition of thin films. Accordingly, applications of this technique range from studies of polymer thin film physics,[14−16] biomaterial properties,[17−19] and block copolymer phase behavior[20−26] to nanoparticle assembly[27] and device fabrication.[28,29] Flowcoating is also popular due to its amenability to high-throughput and combinatorial experiments which leverage the technique's unique capacity to produce films with a thickness gradient.[30−36] This allows for the rapid investigation of the influence of film thickness on properties using only a few samples—sometimes only one. High-throughput approaches like flowcoating thus save time, conserve material, and minimize unintended sample-to-sample variation.

The primary control parameter which dictates film thickness is the coating blade velocity, U. The stage can be made to run at a constant U producing a flat film, not unlike one produced by spin-coating, or the stage can operate with a nonzero acceleration and produce a film with a thickness gradient. To this point, however, the fundamental fluid mechanics which govern this coating process as well as the quantitative relationship between the numerous experimental parameters and the final film profile are yet to be fully understood. Le Berre et al.[37] developed a model for this process using Landau−Levich theory,[38,39] based on the lubrication approximation, which states that the length scale in the direction of the gap is much smaller than the length scale in the flow direction. Landau−Levich theory predicts that all coating flows of this nature should have a solution of the following form:

$$\frac{t_{wet}}{L} = c_1 Ca^{2/3} = c_1\left(\frac{\mu U}{\gamma}\right)^{2/3} \quad (1)$$

where t_{wet} is the coated film thickness far away from the meniscus prior to solvent evaporation, L is a characteristic

Received: April 1, 2014
Revised: May 1, 2014
Published: May 2, 2014

   dx.doi.org/10.1021/la501247x | Langmuir 2014, 30, 5637−5644

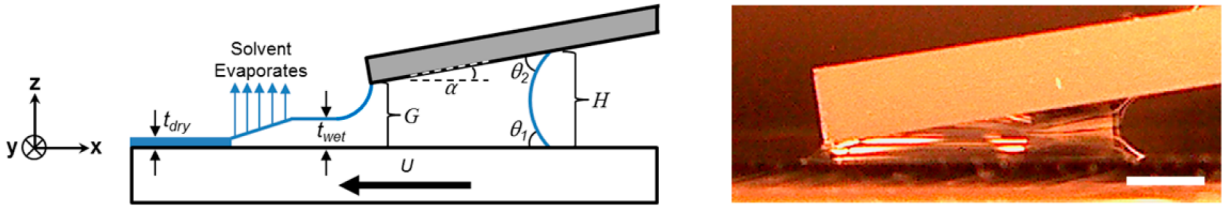

Figure 1. Left: schematic of flowcoating process with relevant experimental parameters labeled. Right: a photograph showing the flowcoater, coating a toluene–polymer solution onto a Si wafer (scale bar indicates 1 mm).

length scale, c_1 is a numerical constant, and *Ca* is the capillary number which is defined in terms of the solution viscosity μ, *U*, and the solution surface tension γ. *Ca* is a dimensionless parameter comparing the relative strength of viscous forces and surface tension in the system.[39] The solution from Le Berre et al. matched this form, with the characteristic length scale *L* identified as the radius of curvature of the rear meniscus *R* and the numerical constant $c_1 = 1.34$. Lau independently solved the problem, yielding a similar solution.[40] Experiments performed by Le Berre and by Lau, all using aqueous solutions or suspensions, showed qualitative agreement with this model, including the proper scaling with *U*. However, the experimental films were typically 2–3 times thicker than the model prediction; this was attributed by Lau to solute-induced Marangoni effects,[41,42] which are known to occur in the presence of surface-active components and can lead to a thickening factor of up to 2.5. If true, then when no surface-active components are present, as is typically the case when coating polymers from organic solvents,[12] this model may indeed provide a useful quantitative guide for the creation of films with desired thicknesses and thickness gradients, though this has yet to be demonstrated.

The purpose of this study is to explore the relationships between the experimental parameters associated with flowcoating and the final polymer film thickness. First, the dependence of film thickness on *U* and *Ca* will be rigorously tested; next, the characteristic length scale proposed by Le Berre and Lau will be examined and used to experimentally determine the prefactor c_1. The result is a design equation which allows a user to produce polymer thin films with precise and broadly tunable film thickness profiles.

EXPERIMENTAL SECTION

Flowcoating. A flowcoater was constructed based on the design by Stafford et al.[12] using a Newport Corp. one-dimensional stage (ILS150CC, maximum velocity = 100 mm/s, maximum acceleration = 400 mm/s^2, on-axis accuracy 5 ± 2.5 μm) and motion controller (ESP300). At one end of the stage a metal holder which can stably mount a glass slide (Fisher precleaned microscope slide, 75 mm × 25 mm × 1 mm, which served as the fixed blade) was placed above the stage. The mount contains four screws, each capable of independently adjusting the blade: the blade height (gap between the substrate and the blade, *G*), blade angle (pitch or angle between the substrate and blade in the direction of motion, α), blade tilt (roll or angle between the substrate and blade in the transverse direction), and the position of the blade in the transverse direction can all be carefully controlled. Figure 1 shows a side-view schematic of the coating process, with all relevant experimental parameters labeled, and a side-view photograph of coating in progress. Additional experimental parameters can be controlled including stage velocity, *U*, and acceleration, *A*, and solution reservoir volume, *V*. These, along with properties of the solution such as polymer concentration, *C*, viscosity, μ, and surface tension, γ, can influence the film thickness.

Materials. Toluene was purchased from EMD Millipore, mixed xylenes were purchased from EM Science, and ethyl acetate and cyclohexane were purchased from Fisher. All solvents were used as received. The following polymers were used in this study: an experimental grade polystyrene (PS) provided by Dow Chemical (M_n = 112 kg/mol, dispersity $Đ$ = 2.8), three additional PS homopolymers synthesized in-house with molecular weights of 16.7 kg/mol ($Đ$ = 1.7), 416 kg/mol ($Đ$ = 1.2), and 1500 kg/mol ($Đ$ = 1.8), poly(methyl methacrylate) (PMMA, M_n = 46.4 kg/mol) and poly(ethylene glycol) (PEG, typical M_n = 8 kg/mol) purchased from Sigma-Aldrich, and two styrene–isoprene–styrene (SIS) triblock copolymers (D1111, 22 wt % PS; D1163, 15 wt % PS) and two styrene–butadiene–styrene (SBS) triblock copolymers (D1102, 28 wt % PS; D1493, 75 wt % PS) provided by Kraton Polymers. PS molecular weights were measured via size exclusion chromotagraphy in tetrahydrofuran calibrated with narrow-distribution PS standards. The polymer solutions were made at the desired concentration (by weight) and stored in a refrigerator. All solutions were allowed to warm to room temperature (20 ± 2 °C) prior to their use in coating experiments. Solvent and solution viscosities at 20 °C were measured via capillary viscometry[43] using a glass Schott-Geräte Ubbelohde dilution viscometer in a temperature-controlled water bath. For a properly sized capillary, the solution flow time is simply proportional to solution viscosity; the flow time of pure toluene, which has a viscosity of 0.59 cP at 20 °C,[44] was used as the reference. Silicon wafers (with native oxide layer), purchased from Silicon Quest, were used as substrates and were liberally washed with toluene prior to use. Contact angles (static, advancing, and receding) were measured using a Ramé-Hart contact angle goniometer, model 500-F1. For all measurements, the droplet mass was approximately 1 mg, and the contact angle was determined using the circle method in the Ramé-Hart software. Tables listing relevant solvent, polymer, and solution properties can be found in the Supporting Information.

Film Preparation and Thickness Measurements. As indicated in Figure 1, the direction of motion is denoted as the *x*-direction, with the *x*-coordinate of the coating gap progressively increasing during coating due to the stage motion; the orthogonal direction in the plane of the substrate is denoted the *y*-direction, and the *z*-direction corresponds to the film thickness. A piece of silicon wafer (approximately 3.0 cm × 6.0 cm) was placed on the stage, beneath the fixed blade. The blade was changed between each coating run. Once positioned, a scratch was made on the substrate to indicate the exact location in *x* on the wafer where coating begins. The gap height and blade angle were then set to the desired values, and the blade was made to be approximately level with the substrate in the *y*-direction. A fixed volume *V* of polymer solution was loaded, via syringe, into the gap where it is held in place by capillary forces, thus creating the solution reservoir. The setup was examined to ensure that the reservoir's contents were evenly distributed along the width of the blade (i.e., uniform distance between front and back menisci). An uneven distribution indicated a need to readjust the *y*-direction blade tilt. The thicknesses of all films produced for this study were measured along *x* at several locations in *y* to ensure uniformity in the *y*-direction (thickness variation in *y* less than 3% of the average film thickness).

After loading the solution, the stage was made to travel the first 3 mm at a constant *U* = 0.1 mm/s, to remove any startup effects the flow may experience. In all figures in this paper, *x* = 0 is taken as the position at the end of this 3 mm constant-velocity travel, regardless of

dx.doi.org/10.1021/la501247x | Langmuir 2014, 30, 5637–5644

the subsequent velocity profile. For typical runs, at $x = 0$ the stage was then programmed to either rapidly accelerate to a constant velocity or to accelerate continuously (with a constant acceleration A) over the remaining length of the substrate (typically 40−50 mm), in both cases depositing a film over the entire substrate. Once coating of the film began, often a moving evaporation front (typically 5−20 mm away from the blade for toluene solutions) could be observed. Subsequently, t_{dry} was measured using a Gaertner Scientific LS116S300 ellipsometer (λ = 632.8 nm) at known positions along the substrate. For films prepared at nonconstant velocity, U was determined from the position (x) along the film using basic equations of motion. Some representative film thickness profiles are shown in Figure 2.

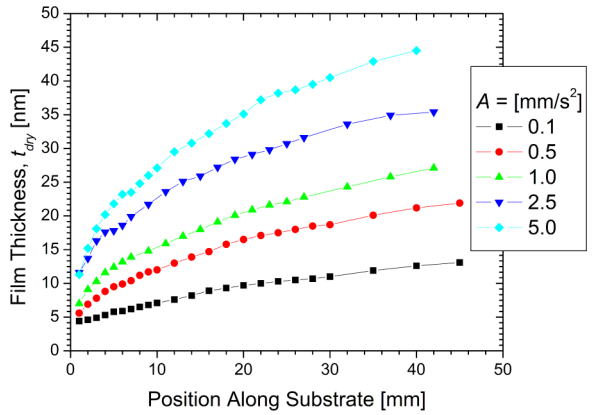

Figure 2. Representative film thickness profiles produced at different constant accelerations, all using a solution of 1 wt % PS (112 kg/mol) in toluene.

The flowcoated films contained negligible quantities of trapped solvent. PS films were flowcoated from toluene at 100 and 200 nm thickness, with the initial thickness measured within an hour of flowcoating; these films were then annealed in air at 150 °C for 30 min, cooled to room temperature, and the thickness remeasured. The 100 nm film showed a thickness decrease of only 0.9%, while the 200 nm film showed a decrease of only 1.6%; analogous spin-coated PS films showed very similar thickness changes following annealing. While these thickness changes represent upper bounds on the minute amount of trapped solvent in the present films, the amount could potentially be larger for solvents of much lower volatility or much stronger affinity for the polymer.

RESULTS AND DISCUSSION

Capillary Number Dependence. Films were deposited from solution (112 kg/mol PS, 1 wt % in toluene) by coating at constant acceleration rates of 0.05, 0.10, 0.50, 1.0, and 5.0 mm/s^2. In addition several films were made with uniform thickness, using a constant U of 0.5, 1.0, 5.0, or 10.0 mm/s. All films were produced with V = 50 μL, G = 200 μm, and $\alpha = 7°$. Figure 3 shows the dry film thickness t_{dry} plotted vs instantaneous coating velocity U on a log−log scale. A best-fit line to the data yields a slope, m = 0.642 ± 0.009 (± indicates one standard deviation), very close to the 2/3 power dependence predicted by Landau−Levich theory. The precise agreement between the flat ($A = 0$) and gradient ($A \neq 0$) films confirms that instantaneous stage velocity, not stage acceleration, is the relevant control parameter.

A wider array of tests was performed by changing the properties of the coating solution: polymer molecular weight and concentration as well as polymer and solvent type (with V, G, and α all still fixed at the previous values). These results are shown in Figure 4. To compare across solutions, the ordinate is

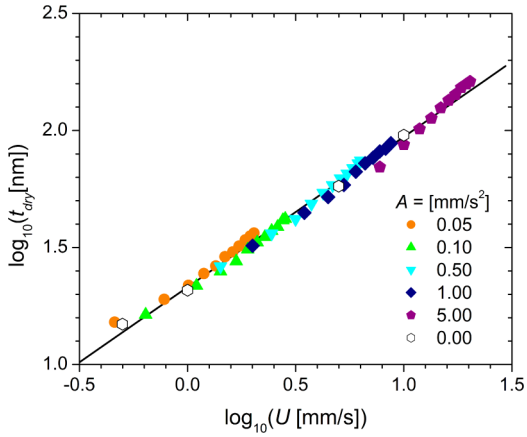

Figure 3. Dry film thickness, t_{dry}, vs stage velocity, U, on a logarithmic scale for a solution of 1 wt % PS (112 kg/mol) in toluene. A best-fit line to the data produces a slope of 0.642 ± 0.009.

plotted in terms of Ca, while the abscissa displays the wet film thickness prior to evaporation, t_{wet}, which was computed from t_{dry} via

$$\frac{t_{dry}}{t_{wet}} = \frac{\frac{w_{polymer}}{\rho_{polymer}}}{\frac{w_{polymer}}{\rho_{polymer}} + \frac{w_{solvent}}{\rho_{solvent}}} \quad (2)$$

where w is the weight fraction of the component in solution and ρ is the density of the pure component. Note that volume additivity is assumed for the solutions, an approximation estimated to be accurate to within 0.1% for the relatively dilute solutions employed here.[45,46] In computing Ca, the viscosity determined by capillary viscometry was used; thus, any shear thinning which may occur at the coating velocity is assumed to be negligible. It was also assumed that the solution surface tension is approximately equal to that of the pure solvent, which should hold as long as total loading of polymer in the solution is low and the polymers are not surface active, which should be the case for the systems studied here (small fractions of polymer dissolved in a good solvent of moderate surface tension).[47]

The data generally appear quite linear on the log−log plots of Figure 4, except at low Ca where some upward curvature is observed. To capture the proper scaling exponent for this coating flow, only data in the linear region ($Ca > 10^{-4}$) were considered when generating best-fit lines; the cause of, and threshold for, the deviations observed at low Ca will be discussed below. The resulting slopes of the best-fit lines are displayed in the corresponding plots in Figure 4. All four panels show a dependence on Ca close to the predicted 2/3 power; moreover, all four panels are essentially identical, as shown by the "master" curve in the Supporting Information, with a best-fit slope of 0.662 ± 0.006. This provides compelling evidence that, in the range of Ca considered ($10^{-4} < Ca < 10^{-2.58}$), the flowcoating process is indeed a Landau−Levich flow and robustly follows the predicted 2/3 dependence.

While velocity (~0.5−20 mm/s) and viscosity (~0.5−5 cP) were each varied over at least a decade in generating the data of Figure 4, one limitation in this work was the comparatively narrow range over which the solution surface tension could be varied (approximately 20%, by changing solvent). Performing experiments over a wide range of γ is difficult, as most organic solvents have comparable surface tensions. In principle,

dx.doi.org/10.1021/la501247x | Langmuir 2014, 30, 5637−5644

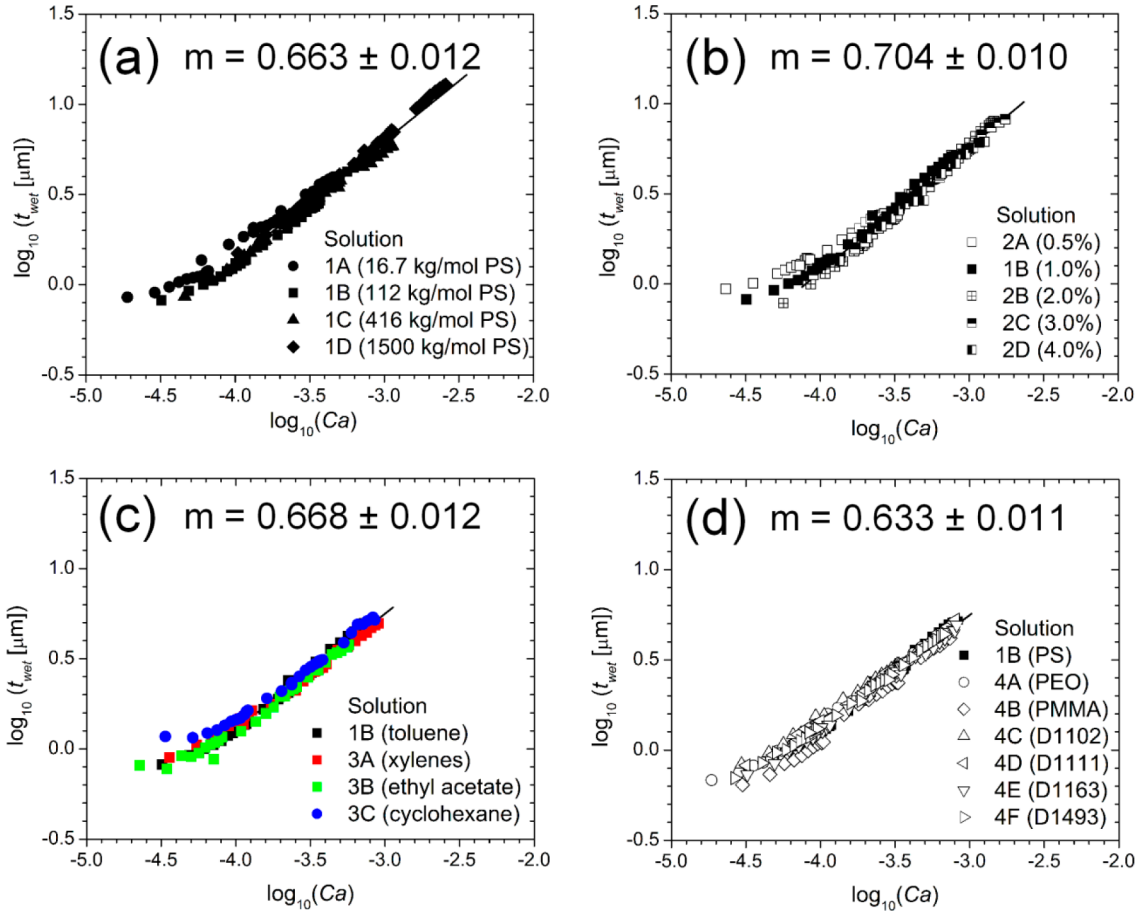

Figure 4. Plots showing t_{wet} vs Ca, where the coating solutions were varied as follows: (a) PS molecular weight, (b) PS concentration, (c) solvent type, and (d) polymer type. Each plot shows the best-fit line (with slope m and ± indicating one standard deviation) for $Ca > 10^{-4}$.

aqueous solutions could also be employed, but considerable effort must be taken to eliminate even trace levels of surfactants; otherwise, Marangoni effects may strongly affect the film thickness.[40]

Characteristic Length Scale. In addition to the 2/3 power dependence of film thickness on Ca, Landau–Levich theory predicts that there should exist a characteristic length scale, L, with which the film thickness should scale linearly; this characteristic length scale depends on the coating geometry.[39] Perhaps surprisingly, both previous work[12] and our own experiments show that the gap height, G, between the blade and the substrate is not a useful predictive length scale in this flow. Instead, the length scale proposed by Le Berre[37] and Lau,[40] derived by calculating the curvature of the static meniscus and using this to obtain a complete solution to the Landau–Levich flow problem, will be used. Because the lateral pressure gradient in the solution reservoir is zero,[37] the radius of curvature in the front and rear menisci can be equated. The rear meniscus height and wetting conditions are typically easier to measure than the curvature; thus, the following expression for the rear meniscus curvature is chosen as the characteristic length scale, L:

$$L = \frac{H}{\cos\theta_1 + \cos\theta_2 - \frac{H^2}{2(l_{cap})^2}} \quad (3)$$

where H is the height of the rear meniscus, θ_1 and θ_2 are the back meniscus wetting angles as shown in Figure 1, and l_{cap} is the capillary length, equal to $\gamma/\rho g$, where g is acceleration due to gravity. The rear meniscus height, H, is somewhat ill-defined and difficult to accurately measure in the experimental setup (with an approximate measurement uncertainty of ~9%). We chose instead to indirectly determine H by approximating the solution reservoir volume as a trapezoidal prism. One can then use simple geometry to compute H from α, G, V, and the blade width, B (here, simply the width of the glass slides used, B = 25 mm).

Although held constant up to this point, V, G, and α may each be varied over some range. Therefore, to test the length scale proposed by eq 3, these parameters were adjusted (20 μL < V < 200 μL, 100 μm < G < 400 μm, 5° < α < 10°) and the calculated H and L were applied in the analysis of the measured film thicknesses according to eq 1. For simplicity, these experiments were all done using one solution (1 wt % of 112 kg/mol PS in toluene), so that θ_1, θ_2, and l_{cap} were not varied. θ_1 and θ_2 were assumed to equal the static contact angles of pure toluene on silicon with native oxide and on glass, respectively. For both substrates, the contact angle was measured to be $\theta_1 = \theta_2 = 15 \pm 4°$ and the contact angle hysteresis (difference between advancing and receding contact angles) was found to be less than the measured error. All flat films were produced using U = 10 mm/s, hence Ca was fixed. Figure 5 shows $t_{wet}/Ca^{2/3}$ vs L for films produced using a variety of G, α, and V. If true Landau–Levich flow is observed, these data should describe a line through the origin with a slope equal to c_1, the numerical constant predicted to be 1.34. The data in

dx.doi.org/10.1021/la501247x | Langmuir 2014, 30, 5637–5644

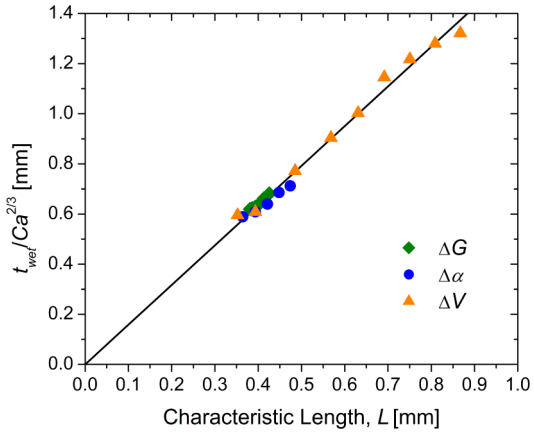

Figure 5. Plot showing $t_{wet}/Ca^{2/3}$ vs the characteristic length scale, L, proposed by eq 3. L was varied by changing the front gap height (ΔG), the blade angle ($\Delta\alpha$), and the solution reservoir volume (ΔV). The slope of the best-fit line, which according to eq 1 should correspond to c_1, equals 1.58 ± 0.02. All films produced using a single solution of 1 wt % PS (112 kg/mol) in toluene.

Figure 5 do indeed conform well to a linear dependence, indicating that film thickness does scale linearly with L; a linear fit yields a slope of 1.58 ± 0.02. The difference between the experimentally determined c_1 and the predicted value (~18%) could reflect the method used to evaluate the rear meniscus height H, wherein the reservoir volume was approximated by a trapezoidal prism. This approach likely underpredicts the true H, leading to an apparent increase in the measured value of c_1. A further consideration is that H has been assumed constant during coating; however, as coating progresses and solution is drawn out, the reservoir volume, and therefore the back meniscus height, gradually decreases. However, calculations suggest that this effect is small for the films of Figures 2−5 (<2% expected change in film thickness); moreover, this effect would actually decrease, not increase, the apparent value of c_1.

Deviations from Landau−Levich Flow at Low Ca. In the preceding analysis, it was assumed that evaporation is negligible during the coating process but then occurs rapidly after coating. Should coating occur too rapidly relative to evaporation, as when using low-volatility solvents, the wet film can flow prior to solvent evaporation, smoothing out the thickness gradient. Conversely, should coating occur too slowly relative to evaporation, one can enter a different coating regime: one which is driven by evaporation rather than Landau−Levich flow.[37,48−52] In the evaporation-dominated regime, film thickness actually decreases in proportion to the stage velocity; the hypothetical wet film thickness prior to

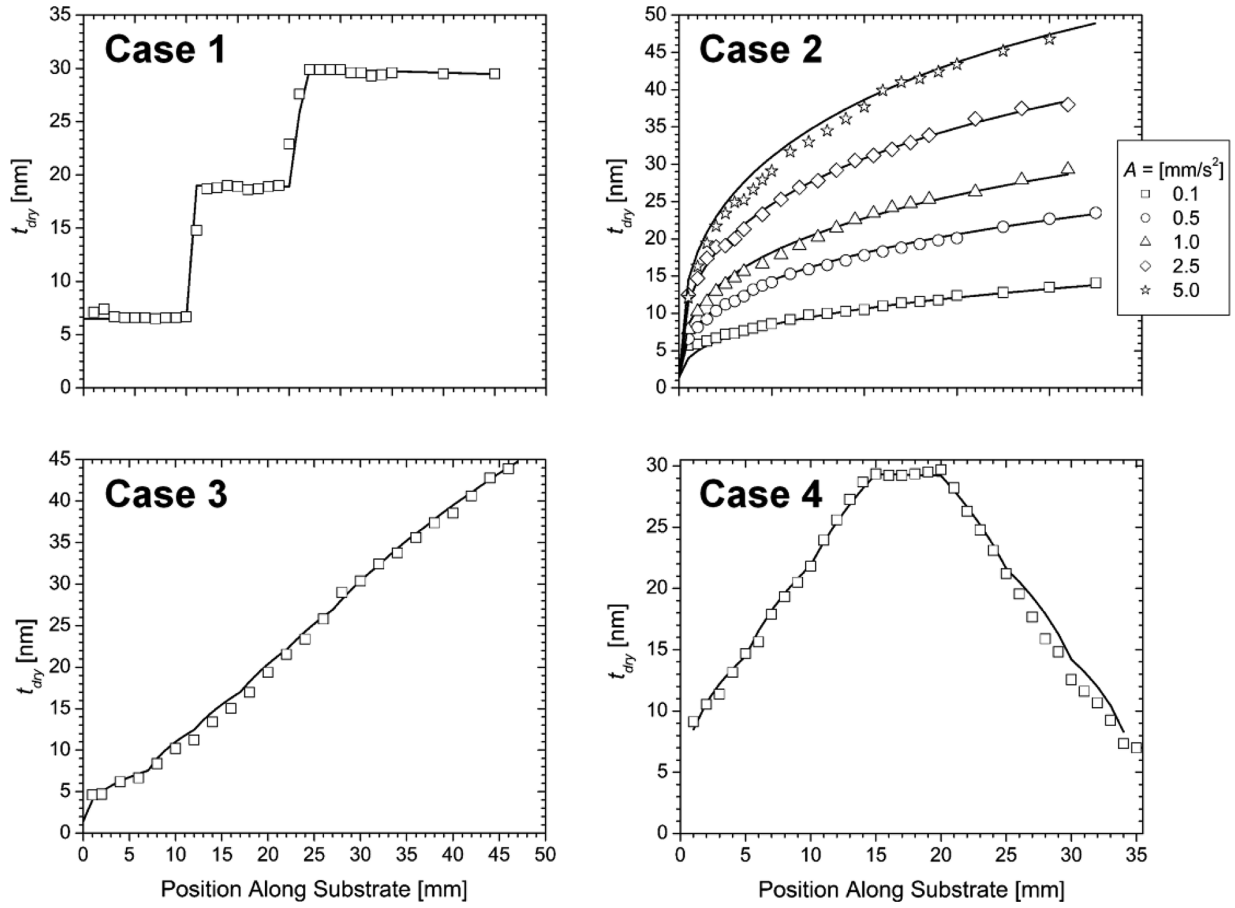

Figure 6. Predicted (lines) and actual (symbols) film thickness vs position profiles. Case 1 (top left) shows rapid increases in velocity from U = 1 mm/s to U = 5 mm/s (at A = 10 mm/s^2) to U = 10 mm/s (at A = 20 mm/s^2). Case 2 (top right) contains profiles generated with constant accelerations of A = 0.1, 0.5, 1.0, 2.5, and 5.0 mm/s^2. Case 3 (bottom left) shows an approximately linear profile with a positive slope created using numerous step increases in acceleration. Case 4 (bottom right) displays a single profile containing sections with positive, zero, and negative thickness gradients. All films were deposited from a solution of 2 wt % PS (112 kg/mol) in toluene.

dx.doi.org/10.1021/la501247x | *Langmuir* 2014, 30, 5637−5644

drying can be determined simply by balancing the rate of evaporation and the rate of coating:

$$t_{wet} = \frac{Q_{evap}}{BU} \tag{4}$$

where Q_{evap} is the volumetric flow rate of the evaporating solvent (as liquid). In this study no attempt was made to systematically investigate the evaporation-dominated regime, as the apparatus is not equipped to control evaporation rate. However, positive deviations from the scaling predicted by eq 1 were observed at low Ca ($<10^{-4}$), which likely indicates an approach to the crossover into the evaporation-driven coating regime. The velocity at which this crossover is expected to occur, U^*, can be predicted by setting eqs 1 and 4 for t_{wet} equal and solving for U:

$$U^* = 0.839\left(\frac{\gamma}{\mu}\right)^{2/5}\left(\frac{Q_{evap}}{BL}\right)^{3/5} \tag{5}$$

Q_{evap} was estimated as the product of the gap height G and blade width B, multiplied by the evaporative flux of toluene [m^3 liquid toluene/m^2s] measured from a full Petri dish placed next to the flowcoater over a fixed time, yielding $Q_{evap} \sim 10^{-12}$ m^3/s. For the toluene solutions used in this study, this yields a range of $U^* \sim 0.1-0.2$ mm/s and range of crossover capillary numbers, Ca^*, $\sim 6 \times 10^{-6}-2 \times 10^{-5}$. While this estimate is only approximate, it suggests that the lowest end of the measured data ($Ca \sim 2 \times 10^{-5}$) may indeed be in the vicinity of the crossover to the evaporation-driven regime. Le Berre showed that for velocities within approximately a factor of 5 of the crossover positive deviations from Landau–Levich scaling can be observed.[37] Therefore, a conservative lower bound above which the data can be expected to be well described by the Landau–Levich model should be $\sim 5/Ca^* = 10^{-4}$, providing the basis for the lower-Ca limit used in the analysis of the data in Figure 4.

Designed Film Profiles. With the successful confirmation of the proposed L and the robust adherence of the film thickness to a $Ca^{2/3}$ dependence, eqs 1 and 3 together constitute the necessary design rules for creating any desired film thickness profile. To test this idea, several complex velocity profiles were programmed and used to deposit films from a 2 wt % solution of 112 kg/mol PS in toluene. The corresponding predicted dry film thickness profiles were then calculated, using the experimentally determined value of $c_1 = 1.58$. In addition, when calculating L from eq 3, a correction to the reservoir volume, V, was applied, decrementing V at any point in the process by the volume of solution used to create the film up to that point. In most cases this correction produces a negligible difference in predicted thickness profile, as in the results of Figures 2–5; however, for the thicker films, this correction was necessary to obtain a precise quantitative match between the model and experiments.

The measured and calculated film thicknesses are displayed in Figure 6. Case 1 depicts a profile which includes several near-step-change increases in stage velocity. Case 2 explores the simple scenario of a constant-acceleration ramp in stage velocity (data are the same as shown in Figure 2). As in case 1, differences between the predicted and measured profiles of no more than 1–2 nm were observed. In the film with $A = 0.1$ mm/s^2, the initial part of the profile does appear flatter and thicker than expected; this can be attributed to the low velocity (and therefore low $Ca < 3 \times 10^{-5}$) at which these films were created, since at $Ca < 10^{-4}$ there are deviations from the predicted Landau–Levich flow due to an approach to the evaporation-driven coating regime. In case 3 an effort was made to produce a roughly linear thickness gradient, by connecting several program segments of varying acceleration (constant A within each segment). Finally, case 4 shows a film with a trapezoidal thickness profile, thus demonstrating the device's ability to controllably produce both positive and negative thickness gradients on a single sample. In total, these four cases illustrate both the precise degree of control attainable using the design rules embodied in eqs 1 and 3 and the broad range of thickness profiles which may be created.

CONCLUSIONS

The flowcoater design by Stafford et al. produces polymer thin films whose thickness is governed by Landau–Levich flow: the film thickness scales with $Ca^{2/3}$ and is proportional to a characteristic length scale L which is dictated by the height of the rear meniscus (through the solution reservoir volume, blade tilt angle, and gap height) and the contact angles of the solution on the blade and substrate. Numerous coating solutions prepared from different polymers and organic solvents all yielded film thicknesses in excellent quantitative accord with the model, thus displaying the versatility of the method. Additionally, the scaling holds true over a wide range of Ca and t_{dry} (over an order of magnitude in both cases), though deviations from the model are observed for $Ca < 10^{-4}$ as the evaporation-driven coating regime is approached. Most importantly, this rigorously tested model can now be used as a design equation, enabling the user to create polymer films with tailored thickness gradients. These results should allow for more convenient and widespread use of this device for a variety of polymer thin film experiments, especially studies which can benefit from the combinatorial potential offered by thickness-gradient films.

ASSOCIATED CONTENT

Supporting Information

Tables showing the relevant properties of all solvents, polymers, and solutions used in this work as well as a "master" plot containing all the data from Figure 4. This material is available free of charge via the Internet at http://pubs.acs.org.

AUTHOR INFORMATION

Corresponding Author

*Tel +1 609 258 4691; fax +1 609 258 0211; e-mail register@princeton.edu (R.A.R.).

Notes

The authors declare no competing financial interest.

ACKNOWLEDGMENTS

The authors gratefully acknowledge helpful discussions with Cindy Lau, William Russel, and Howard Stone and generous financial support from the National Science Foundation, Materials Research Science and Engineering Center (MRSEC) Program, through the Princeton Center for Complex Materials (DMR-0819860).

REFERENCES

(1) Zelikin, A. N. Drug Releasing Polymer Thin Films: New Era of Surface-Mediated Drug Delivery. *ACS Nano* **2010**, *4*, 2494–2509.

(2) Ai, H.; Jones, S. A.; Lvov, Y. M. Biomedical Applications of Electrostatic Layer-by-Layer Nano-Assembly of Polymers, Enzymes, and Nanoparticles. *Cell Biochem. Biophys.* **2003**, *39*, 23−43.
(3) Stuart, M. A. C.; Huck, W. T. S.; Genzer, J.; Müller, M.; Ober, C.; Stamm, M.; Sukhorukov, G. B.; Szleifer, I.; Tsukruk, V. V.; Urban, M.; Winnik, F.; Zauscher, S.; Luzinov, I.; Minko, S. Emerging Applications of Stimuli-Responsive Polymer Materials. *Nat. Mater.* **2010**, *9*, 101−113.
(4) Arias, A. C.; MacKenzie, J. D.; McCulloch, I.; Rivnay, J.; Salleo, A. Materials and Applications for Large Area Electronics: Solution-Based Approaches. *Chem. Rev.* **2010**, *110*, 3−24.
(5) Black, C. T.; Ruiz, R.; Breyta, G.; Cheng, J. Y.; Colburn, M. E.; Guarini, K. W.; Kim, H. C.; Zhang, Y. Polymer Self Assembly in Semiconductor Microelectronics. *IBM J. Res. Dev.* **2007**, *51*, 605−633.
(6) Hall, D. B.; Underhill, P.; Torkelson, J. M. Spin Coating of Thin and Ultrathin Polymer Films. *Polym. Eng. Sci.* **1998**, *38*, 2039−2045.
(7) Yang, C. C.; Josefowicz, J. Y.; Alexandru, L. Deposition of Ultrathin Films by a Withdrawal Method. *Thin Solid Films* **1980**, *74*, 117−127.
(8) Hammond, P. T. Form and Function in Multilayer Assembly: New Applications at the Nanoscale. *Adv. Mater.* **2004**, *16*, 1271−1293.
(9) Usiu, H. Preparation of Polymer Thin Films by Physical Vapor Deposition. In *Functional Polymer Films*; Knoll, W., Advincula, R. C., Eds.; Wiley-VCH: Weinheim, Germany, 2011; Vol. *1*, pp 287−318.
(10) Ozaydin-Ince, G.; Coclite, A. M.; Gleason, K. K. CVD of Polymeric Thin Films: Applications in Sensors, Biotechnology, Microelectronics/Organic Electronics, Microfluidics, MEMS, Composites and Membranes. *Rep. Prog. Phys.* **2012**, *75*, 1−40.
(11) Shepard, K. B.; Priestley, R. D. MAPLE Deposition of Macromolecules. *Macromol. Chem. Phys.* **2013**, *214*, 862−872.
(12) Stafford, C. M.; Roskov, K. E.; Epps, T. H., III; Fasolka, M. J. Generating Thickness Gradients of Thin Polymer Films via Flow Coating. *Rev. Sci. Instrum.* **2006**, *77*, 023908.
(13) Singh, G.; Batra, S.; Zhang, R.; Yuan, H.; Yager, K. G.; Cakmak, M.; Berry, B.; Karim, A. Large-Scale Roll-to-Roll Fabrication of Vertically Oriented Block Copolymer Thin Films. *ACS Nano* **2013**, *7*, 5291−5299.
(14) Huang, H.; Chung, J. Y.; Nolte, A. J.; Stafford, C. M. Characterizing Polymer Brushes via Surface Wrinkling. *Chem. Mater.* **2007**, *19*, 6555−6560.
(15) Lee, J. H.; Thio, B. J. R.; Bae, T. H.; Meredith, J. C. Role of Lewis Basicity and van der Waals Forces in Adhesion of Silica MFI Zeolites (010) with Polyimides. *Langmuir* **2009**, *25*, 9101−9107.
(16) Roskov, K. E.; Epps, T. H., III; Berry, B. C.; Hudson, S. D.; Tureau, M. S.; Fasolka, M. J. Preparation of Combinatorial Arrays of Polymer Thin Films for Transmission Electron Microscopy Analysis. *J. Comb. Chem.* **2008**, *10*, 966−973.
(17) Aamer, K. A.; Genson, K. L.; Kohn, J.; Becker, M. L. Impact of Polymer-Bound Iodine on Fibronectin Adsorption and Osteoblast Cell Morphology in Radiopaque Medical Polymers: Tyrosine-Derived Polycarbonate Blends as a Model System. *Biomacromolecules* **2009**, *10*, 2418−2462.
(18) Chang, R. C.; Johnson, P.; Stafford, C. M.; Hwang, J. Fabrication and Characterization of a Multilayered Optical Tissue Model with Embedded Scattering Microspheres in Polymeric Materials. *Biomed. Opt. Express* **2012**, *3*, 1326−1339.
(19) Chen, R.; Gallant, N.; Smith, J.; Kipper, M.; Simon, C., Jr. Time-Dependent Effects of Pre-Aging Polymer Films in Cell Culture Medium on Cell Adhesion and Spreading. *J. Mater. Sci.: Mater. Med.* **2008**, *19*, 1759−1766.
(20) Albert, J. N. L.; Baney, M. J.; Stafford, C. M.; Kelly, J. Y.; Epps, T. H., III Generation of Monolayer Gradients in Surface Energy and Surface Chemistry for Block Copolymer Thin Film Studies. *ACS Nano* **2009**, *3*, 3977−3986.
(21) Albert, J. N. L.; Bogart, T. D.; Lewis, R. L.; Beers, K. L.; Fasolka, M. J.; Hutchison, J. B.; Vogt, B. D.; Epps, T. H., III Gradient Solvent Vapor Annealing of Block Copolymer Thin Films Using a Microfluidic Mixing Device. *Nano Lett.* **2011**, *11*, 1351−1357.
(22) Albert, J. N. L.; Young, W.-S.; Lewis, R. L.; Bogart, T. D.; Smith, J. R.; Epps, T. H., III Systematic Study on the Effect of Solvent Removal Rate on the Morphology of Solvent Vapor Annealed ABA Triblock Copolymer Thin Films. *ACS Nano* **2011**, *6*, 459−466.
(23) Epps, T. H., III; DeLongchamp, D. M.; Fasolka, M. J.; Fischer, D. A.; Jablonski, E. L. Substrate Surface Energy Dependent Morphology and Dewetting in an ABC Triblock Copolymer Film. *Langmuir* **2007**, *23*, 3355−3362.
(24) Yager, K. G.; Fredin, N. J.; Zhang, X.; Berry, B. C.; Karim, A.; Jones, R. L. Evolution of Block-Copolymer Order Through a Moving Thermal Zone. *Soft Matter* **2010**, *6*, 92−99.
(25) Zhang, X.; Berry, B. C.; Yager, K. G.; Kim, S.; Jones, R. L.; Satija, S.; Pickel, D. L.; Douglas, J. F.; Karim, A. Surface Morphology Diagram for Cylinder-Forming Block Copolymer Thin Films. *ACS Nano* **2008**, *2*, 2331−2341.
(26) Zhang, X.; Yager, K. G.; Fredin, N. J.; Ro, H. W.; Jones, R. L.; Karim, A.; Douglas, J. F. Thermally Reversible Surface Morphology Transition in Thin Diblock Copolymer Films. *ACS Nano* **2010**, *4*, 3653−3660.
(27) Mittal, M.; Niles, R. K.; Furst, E. M. Flow-Directed Assembly of Nanostructured Thin Films from Suspensions of Anisotropic Titania Particles. *Nanoscale* **2010**, *2*, 2237−2243.
(28) Cho, W.; Kim, T.; Char, K.; Soles, C. L. A Facile Method for the Preferential Alignment of Mesochannels in Silica Films by Solution Flow. *Microporous Mesoporous Mater.* **2010**, *131*, 136−140.
(29) Sakamoto, K.; Ueno, J.; Bulgarevich, K.; Miki, K. Anisotropic Charge Transport and Contact Resistance of 6,13-bis-(triisopropylsilylethynyl) Pentacene Field-Effect Transistors Fabricated by a Modified Flow-Coating Method. *Appl. Phys. Lett.* **2012**, *100*, 123301.
(30) Aamer, K. A.; Stafford, C. M.; Richter, L. J.; Kohn, J.; Becker, M. L. Thin Film Elastic Modulus of Degradable Tyrosine-Derived Polycarbonate Biomaterials and Their Blends. *Macromolecules* **2009**, *42*, 1212−1218.
(31) Li, X.; Vogt, B. D. Impact of Thickness on CO_2 Concentration Profiles Within Polymer Films Swollen Near the Critical Pressure. *Polymer* **2009**, *50*, 4182−4188.
(32) Luo, M.; Seppala, J.; Albert, J. N.; Lewis, R., III; Mahadevapuram, N.; Stein, G.; Epps, T. H., III Manipulating Nanoscale Morphologies in Cylinder-Forming Poly(styrene-b-isoprene-b-styrene) Thin Films Using Film Thickness and Substrate Surface Chemistry Gradients. *Macromolecules* **2013**, *46*, 1803−1811.
(33) Papalia, J. M.; Marencic, A. P.; Adamson, D. H.; Chaikin, P. M. Register, R. A. Thin Films of Block Copolymer-Homopolymer Blends with a Continuously Tunable Density of Spherical Microdomains. *Macromolecules* **2010**, *43*, 6946−6949.
(34) Rathfon, J. M.; Cohn, R. W.; Crosby, A. J.; Rothstein, J. P.; Tew, G. N. Confinement Effects on Chain Entanglement in Free-Standing Polystyrene Ultrathin Films. *Macromolecules* **2011**, *44*, 5436−5442.
(35) Sohn, K. E.; Kojio, K.; Berry, B. C.; Karim, A.; Coffin, R. C.; Bazan, G. C.; Kramer, E. J.; Sprung, M.; Wang, J. Surface Effects on the Thin Film Morphology of Block Copolymers with Bulk Order-Order Transitions. *Macromolecules* **2010**, *43*, 3406−3414.
(36) Yager, K. G.; Berry, B. C.; Page, K.; Patton, D.; Karim, A.; Amis, E. J. Disordered Nanoparticle Interfaces for Directed Self-Assembly. *Soft Matter* **2009**, *5*, 622−628.
(37) Le Berre, M.; Chen, Y.; Baigl, D. From Convective Assembly to Landau−Levich Deposition of Multilayered Phospholipid Films of Controlled Thickness. *Langmuir* **2009**, *25*, 2554−2557.
(38) Landau, L.; Levich, B. Dragging of a Liquid By a Moving Plate. *Acta Physicochim. USSR* **1942**, *17*, 42−54.
(39) Stone, H. A. Interfaces: In Fluid Mechanics and Across Disciplines. *J. Fluid Mech.* **2010**, *645*, 1−25.
(40) Lau, C. Y. C. Formation and Order Enhancement of Submicrometer and Nanoscale Features in Thin Films. Ph.D. Thesis, Princeton University, Sept 2013.
(41) Fanton, X.; Cazabat, A. M. Spreading and Instabilities Induced by a Solutal Marangoni Effect. *Langmuir* **1998**, *14*, 2554−2561.

(42) Ramdane, O. O.; Quere, D. Thickening Factor in Marangoni Coating. *Langmuir* **1997**, *13*, 2911−2916.
(43) Ubbelohde, L. The Principle of the Suspended Level: Applications to the Measurement of Viscosity and Other Properties of Liquids. *Ind. Eng. Chem., Anal. Ed.* **1937**, *9*, 85−90.
(44) Santos, F. J.; Nieto de Castro, C. A.; Dymond, J. H.; Dalaouti, N. K.; Assael, M. J.; Nagashima, A. Standard Reference Data For the Viscosity of Toluene. *J. Phys. Chem. Ref. Data* **2006**, *35*, 1−8.
(45) Bianchi, U.; Cuniberti, C.; Pedemonte, E.; Rossi, C. Conformational Energy Contribution to the Heat of Solution in Polymer-Solvent Systems. Part II. Experimental Results. *J. Polym. Sci., Part A-2* **1969**, *7*, 855−866.
(46) Scholte, T. G. Determination of Thermodynamic Parameters of Polymer-Solvent Systems from Sedimentation-Diffusion Equilibrium in the Ultracentrifuge. *J. Polym. Sci., Part A-2* **1970**, *8*, 841−868.
(47) Ober, R.; Paz, L.; Taupin, C.; Pincus, P.; Boileau, S. Study of the Surface Tension of Polymer Solutions: Theory and Experiments. Good Solvent Conditions. *Macromolecules* **1983**, *16*, 50−55.
(48) Brinker, C. J.; Lu, Y.; Sellinger, A.; Fan, H. Evaporation-Induced Self-Assembly: Nanostructures Made Easy. *Adv. Mater.* **1999**, *11*, 579−585.
(49) Deegan, R. D.; Bakajin, O.; Dupont, T. F.; Huber, G.; Nagel, S. R.; Witten, T. A. Capillary Flow as the Cause of Ring Stains From Dried Liquid Drops. *Nature* **1997**, *389*, 827−829.
(50) Kumnorkaew, P.; Ee, Y.-K.; Tansu, N.; Gilchrist, J. F. Investigation of the Deposition of Microsphere Monolayers for Fabrication of Microlens Arrays. *Langmuir* **2008**, *24*, 12150−12157.
(51) Prevo, B. G.; Velev, O. D. Controlled, Rapid Deposition of Structured Coatings From Micro- and Nanoparticle Suspensions. *Langmuir* **2004**, *20*, 2099−2107.
(52) Yabu, H.; Shimomura, M. Preparation of Self-Organized Mesoscale Polymer Patterns on a Solid Substrate: Continuous Pattern Formation from a Receding Meniscus. *Adv. Funct. Mater.* **2005**, *15*, 575−581.